Adam Mickiewicz University, Poznań

Gaia DR3 and colors of the Solar System

The Milky Way Revealed by Gaia: The Next Frontier

Dagmara Oszkiewicz
dagmara.oszkiewicz@amu.edu.pl

Adam Mickiewicz University in Poznań, Poland

September 4, 2023

Introduction

Taxonomic schemes

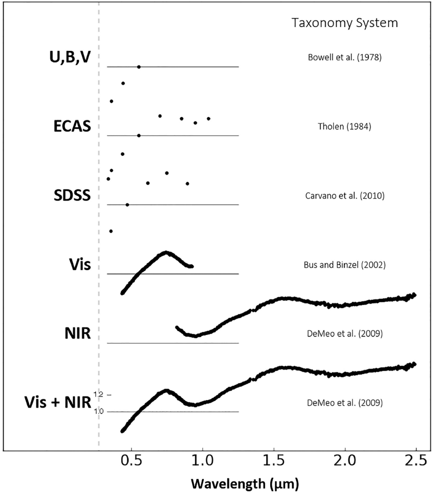

Binzel et al. 2019

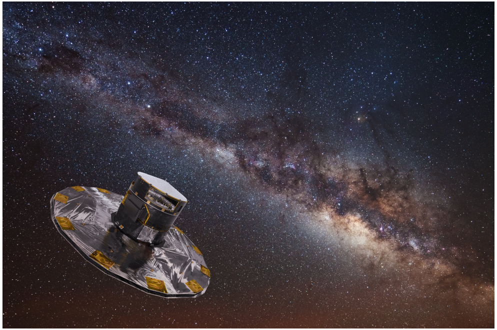

ESA (www.esa.int)

- 60 518 objects
- 16 points every 0.044μm
- coverage: 0.374μm - 1.05μm
- extending more into UV then the typical ground-based spectra

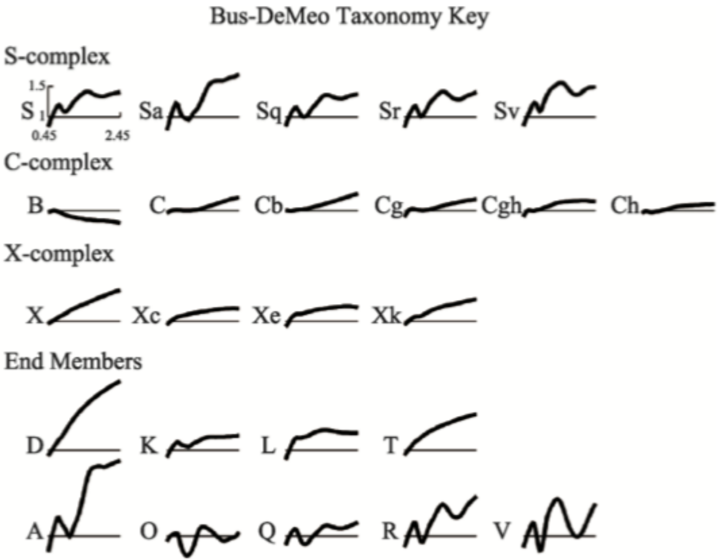

http://smass.mit.edu/busdemeoclass.html F.E.DeMeo,R.P.Binzel, S.M.Slivan, and S.J.Bus.Icarus 202（2009）160-180

Introduction

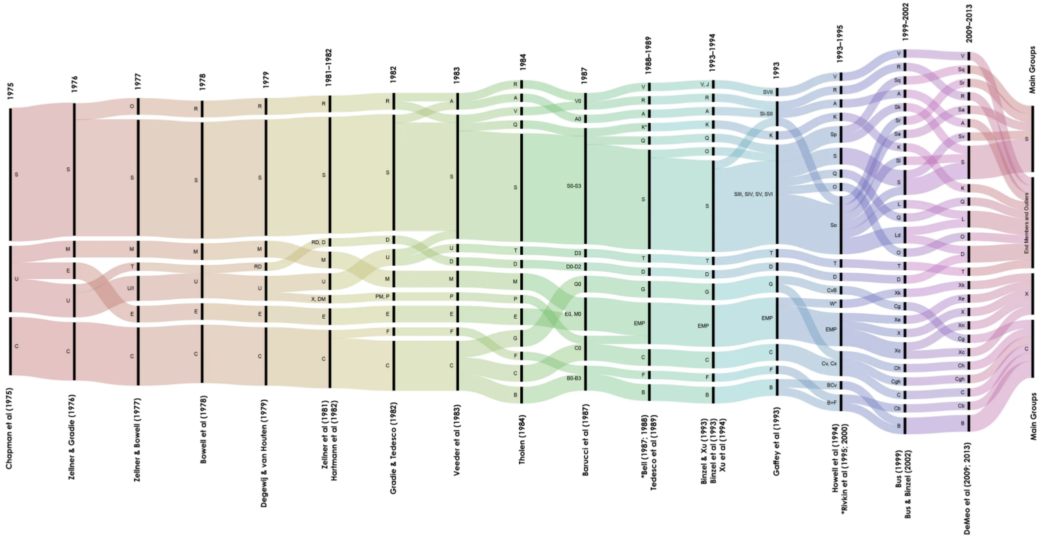

Figure from vissiniti.com

The compositional mass distribution throughout the asteroid belt out to the Trojans.

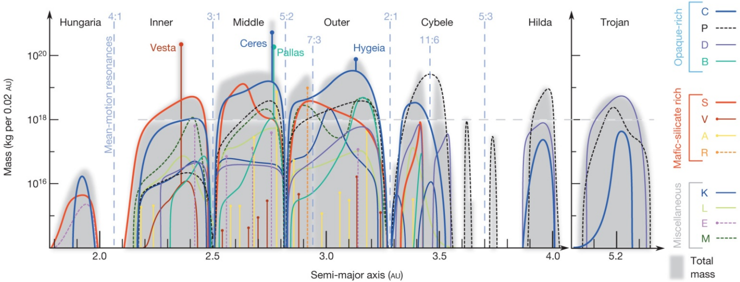

FE DeMeo & B Carry *Nature* **505**, 629-634 (2014) doi:10.1038/nature12908

Cartoon of the effects of planetary migration on the asteroid belt.

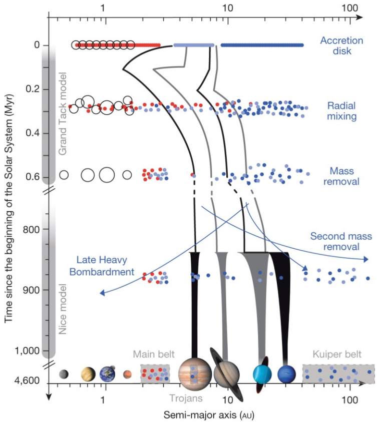

FE DeMeo & B Carry *Nature* **505**, 629-634 (2014) doi:10.1038/nature12908

DR3 spectra

Asteroid spectra in DR3 (Galluccio et al. [1]):

- 60 518 objects
- blue and red photometers (BP/RP)
- spectra is averaged over multiple transits/epochs
- 16 points every 0.044μm
- coverage: 0.374μm - 1.05μm
- wavelength, reflectance_spectrum, reflectance_spectrum_err, reflectance_spectrum_flag (poor quality or compromised)
- most spectra taken at 10-30 deg of phase angle

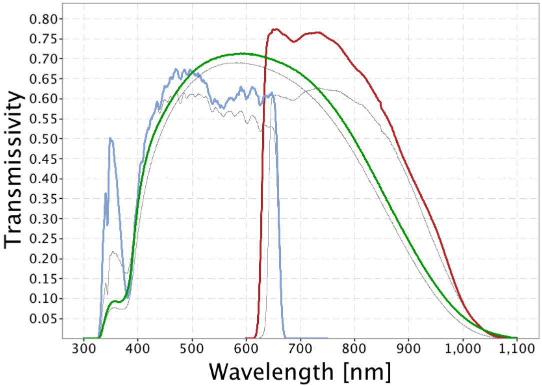

Figure: Passbands for G (green), GBP (blue) and GRP (red). The thin, grey lines show the nominal, pre-launch passbands published in Jordi et al. 2010 [5], used for Gaia DR1. Image from `https://www.cosmos.esa.int`

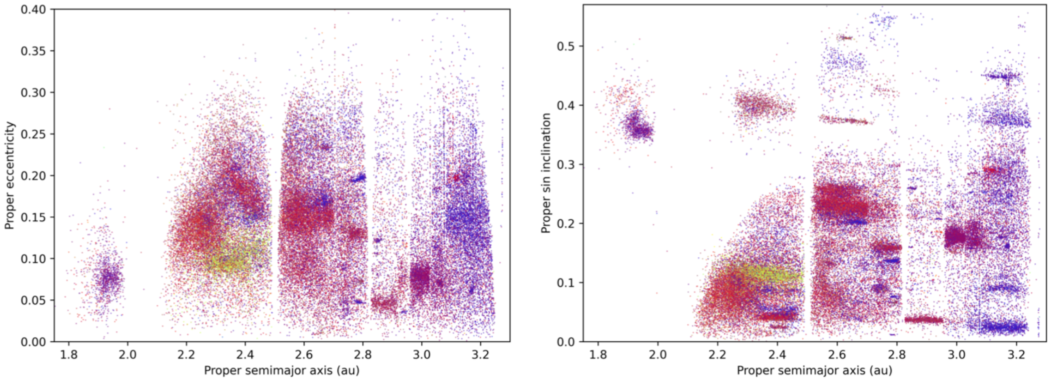

Fig. 12. Plot of the proper semi-major axis vs. proper eccentricity and sin of proper inclination for *Gaia* DR3 SSOs of the main-belt and Hungaria region. The colour of each dot is representative of the object's colour measured by *Gaia* according to the colour scheme defined in Section 4.2.

Gaia Collaboration, Galuccio et al. 2023
Color codding according to the position in the i-z vs. slope plot. S-complex is red to brown, C-complex blue, V-types green, D- and L- are red, X- and K-types magenta.

Family ages

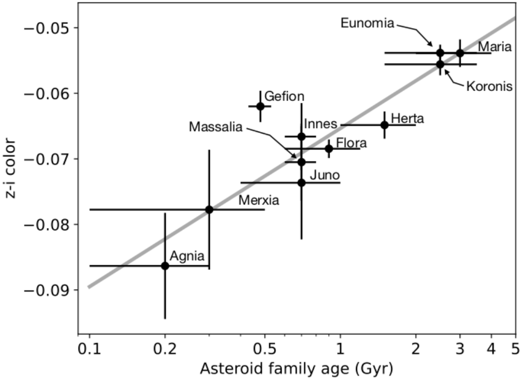

Gaia Collaboration, Galuccio et al. 2023

Galuccio et al. 2023:

- Correlation between z-i colour and the logarithm of the family age has a correlation coefficient of 0.91
- Correlation between spectral slope and the log of family age has a correlation coefficient 0.67
- weak correlation between phase angle and spectral slope (0.3) and between phase angle and depth of the 0.9 micron band (-0.1) for S-complex asteroids

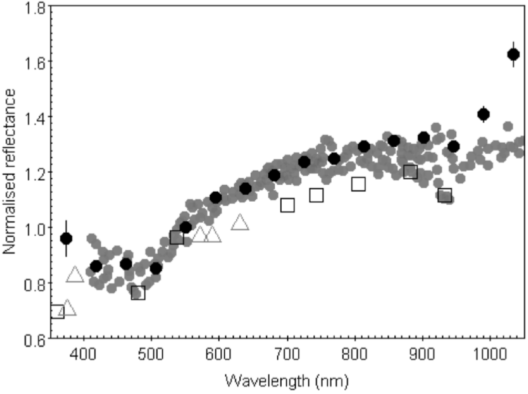

Fig. 19. *Gaia* mean reflectance spectrum of the asteroid (2867) Šteins, shown with black circles together with literature ground-based spectra from Barucci et al. (2005), with grey circles, and data obtained in space by the ESA Rosetta mission using OSIRIS NAC, black open squares, and OSIRIS WAC, black open upside-down triangle (phase angles between 0 and 132°, Keller et al. 2010).

Galuccio et al. 2023

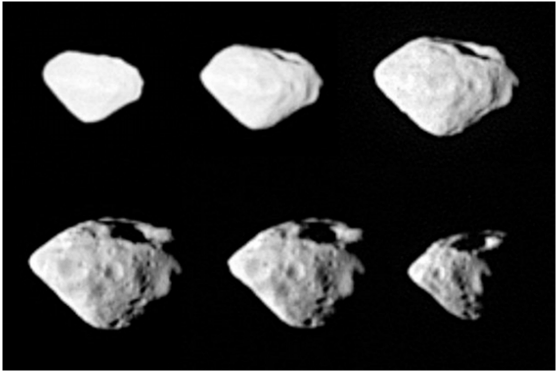

ESA: Images of asteroid (2867) Steins taken by the OSIRIS Wide Angle Camera on Rosetta during the fly-by of 5 September 2008. Credit: ESA 2008 MPS for OSIRIS Team MPS/UPD/LAM/IAA/RSSD/ INTA/UPM/DASP/IDA

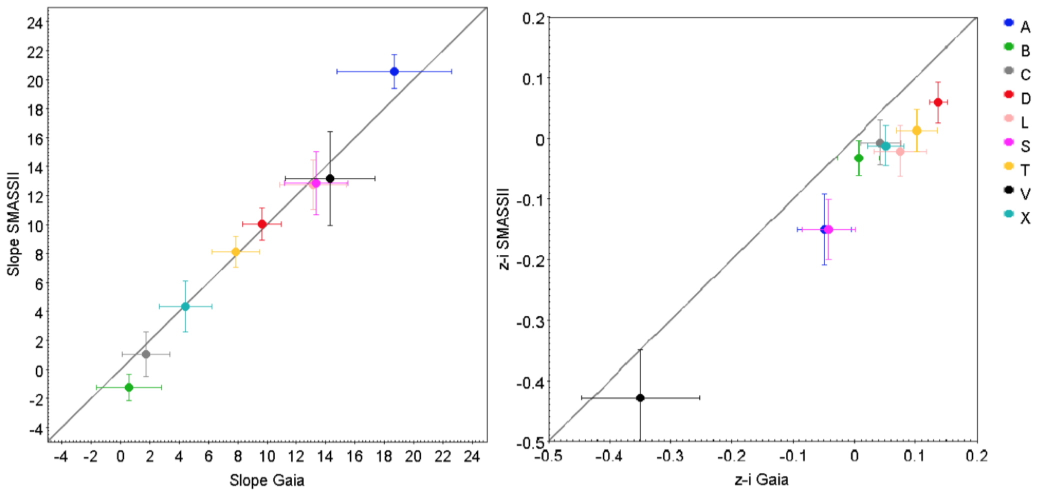

Fig. 10. Comparison of mean spectral slopes and mean z-i colours of different taxonomic classes calculated on asteroids in common between *Gaia* DR3 and the SMASSII survey.

Galuccio et al. 2023

F. Tinaut-Ruano et al.: Asteroids' reflectance from *Gaia* DR3: Artificial reddening at near-UV wavelengths

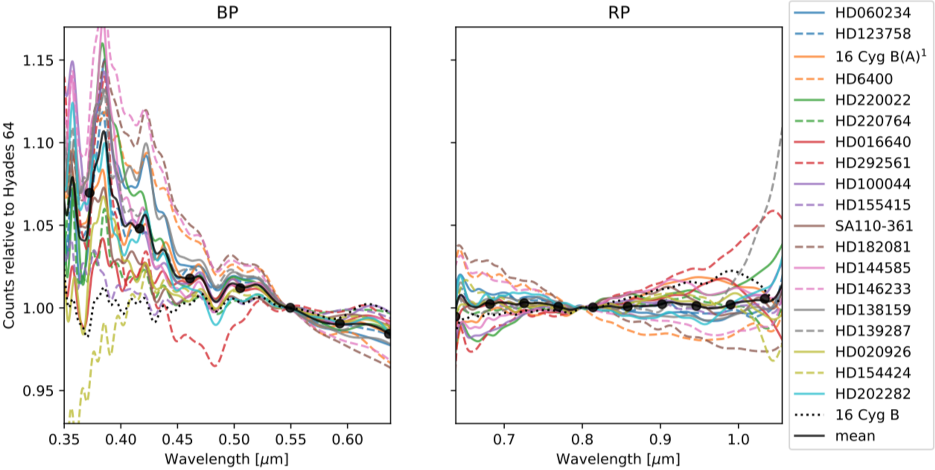

Fig. 1. Ratio between the internally calibrated spectra of each of the *Gaia* SAs and Hyades 64 in the blue photometer (BP, left panel) and the red photometer (RP, right panel). We also plotted the ratio of the mean *Gaia* SA and Hyades 64 (black solid line) and the binned version of this ratio at the wavelengths provided for SSO in *Gaia* DR3 (black dots). [1] We note that the star identified as 16 Cygnus B in Gaia Collaboration (2022) is in fact 16 Cyg A (see the main text for more details).

Tinaut-Ruano et al. 2023

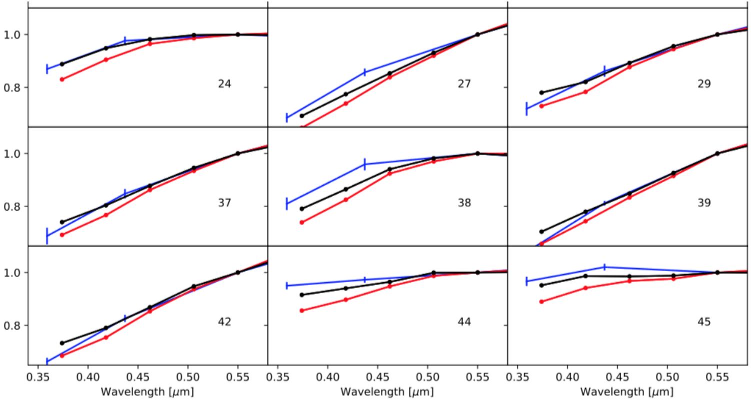

Fig. A.1. Comparison between ground-based observations from the Eight Asteroid Survey (ECAS, dark blue line), TNG observations (light blue line) original *Gaia* data (red line), and corrected data (black line). We also included a UV spectrum of asteroid (624) downloaded from ESA archive and obtained with the instrument STIS, on board the Hubble Space Telescope (HST).

Tinaut-Ruano et al. 2023

DR3 vs. ground-based spectra for V-type asteroids

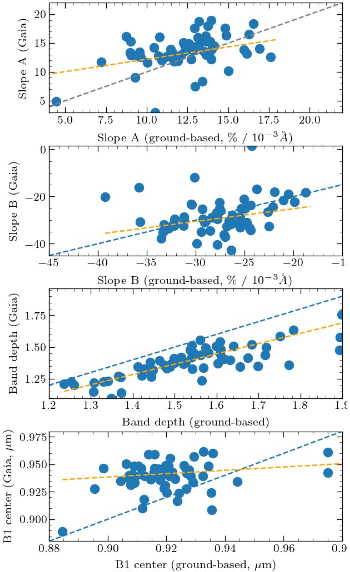

Comparison of spectral slopes, band depths and centers for ground-based and Gaia observations of V-type asteroids. The dashed blue and orange lines represent the 1:1 relation, and a linear regression on the sample, respectively.

- Slope A - the reflectance gradient in the 0.5μm-0.75μm range
- Slope B - the reflectance gradient in the 0.8μm-0.92μm range
- Apparent depth - the ratio between reflectance at 0.75μm and 0.9μm
- Center of the 0.9 μm absorption band

DR3 should be internally consistent.

Training dataset

- We perform **binary classification** into two categories: V-type vs. other types
- Collection of 3057 taxonomic labels from Mahlke et al 2022 [6]
- Labels are cross-matched with objects observed by the mission leading to a sample containing **149 V-types and 2908 other-type asteroids**.
- We omit reflectances at the wavelengths of 0.374, 0.418, 0.990, and 1.034 μm, as they are known to be affected by large random and systematic errors [1]
- We used **slope and slope-removed validated reflectances at the 12 wavelengths**

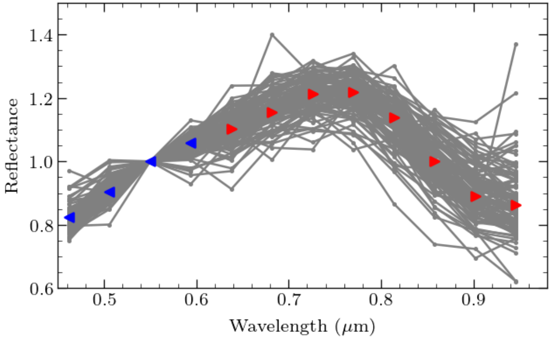

Figure: Spectra of 149 V-type asteroids used in the training process and their averaged spectra from the BP (blue) and RP (red) spectrometers.

Methods

- **Gradient Boosting (GB)** is a set of weak prediction methods. In particular, we use several decision trees. In each iteration, a new model is trained to minimize the residual left from the estimator from the previous stage elements-of-statistical-learning.
- **Support Vector Machines (SVM)** divide the feature space of different classes into separate regions with hyperplanes elements-of-statistical-learning. The algorithm maximises the width of the gap between the different classes.
- **Multilayer Perceptrons (MLP)** is a feedforward artificial neural network with two or three layers of perceptrons, each with 32 or 64 neurones. The weights of the neural connections are adjusted in a learning process with rates between 0.01 and 0.1 [2]. We adjust the network for -type input and use a binary classification.

To evaluate the algorithms, we use a balanced accuracy metric:

$$\mathrm{BAcc} = \frac{1}{k}\sum_{i=1}^{k} \frac{TP_i}{TP_i + FN_i}$$

where k is the number of classes, TP_i ("true positives") is the number of correctly classified objects of class i, FP_i ("false positives") is the number of objects incorrectly classified in class i and FN_i ("false negatives") the number of incorrectly classified objects from class i.

To estimate the accuracy of the method, we use a 5-fold validation. That is, we divide the training set into 5 random parts. The algorithms are trained in 4 parts and evaluated in the 5th part. This process is repeated five times.

Results

Balanced accuracy was 92%, 92%, and 91% for GB, SVM and MLP. Some miss-classification occurs for Q/S-complex asteroids and objects with poor quality spectra as well as some rare types with 0.9μm band such as A-, R-, O-type.

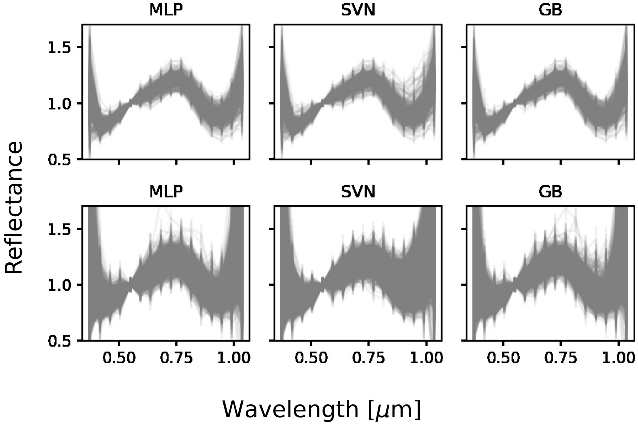

Figure: Spectra of all the classified as V-types in the validated (top) and full sample (bottom).

Populations

We further split the two data sets into different populations in a consistent way with the literature [4, 3] based on orbital parameters, semi-major axis *a*, eccentricity *e*, and inclination *i*:

- **Inner main-Belt** (2.1 au $<$ a $\leq$ 2.5 au):
  - **Vestoids** - members of the dynamical Vesta family as defined by the hierarchical clustering method by [7]
  - **Fugitives** - objects outside the dynamical Vesta family having 2.1 au $<$ a $\leq$ 2.3 au, 5 $<$ i $<$ 8, and 0.035 $<$ e $<$ 0.162
  - **Low-i** - objects outside the dynamical Vesta family having 2.3 au $<$ a $\leq$ 2.5 au and i < 6
  - **Phocaea** - with inclination above the ν_6 resonance, 2.5 au $>$a$>$2.25 au, e$>$0.1 and 32>i>18
  - **Hungaria** 2.0 au $>$a$>$1.78 au, 32$>$i$>$16, e$<$0.18
  - **Inner other** - remaining objects in the inner main-Belt
- **Middle main-Belt** (2.5 au $<$ a $\leq$ 2.82 au)
- **Other main-Belt** (2.82 au $<$ a $<$ 3.2 au)

Results

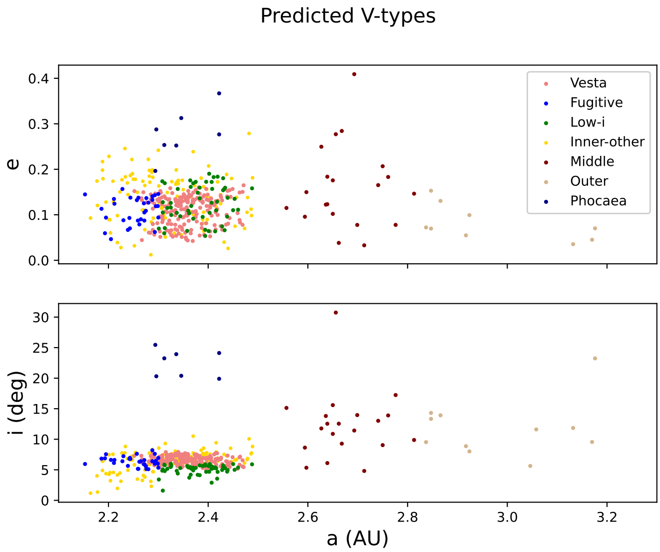

Predicted V-types
Vesta
Fugitive
Low-i
Inner-other
Middle
Outer
Phocaea
e
0.0
0.1
0.2
0.3
0.4
i (deg)
0
5
10
15
20
25
30
2.2
2.4
2.6
2.8
3.0
3.2
a (AU)

Results

Population/Method	MLP	SVM	GB
Vesta	170 (907)	155 (853)	153 (762)
Fugitive	31 (187)	25 (157)	31 (156)
Low-i	47 (267)	49 (293)	46 (231)
Inner-other	105 (582)	104 (594)	98 (507)
Middle	16 (27)	19 (242)	16 (35)
Outer	10 (15)	10 (74)	7 (15)
Hungaria	0 (1)	0 (6)	0 (0)
Phocaea	5 (9)	4 (28)	3 (4)

Table: The total number of new classified V-types in the validated and full sample (in brackets) per population.

- Additional visual validation for Middle, Outer main-Belt and the Phocaea and Hungaria regions.
- SVN seems to have problems with separating the two categories of objects and predicting the correct type especially for noisy/low quality data

Results - spectra of predicted V-types in the outer belt

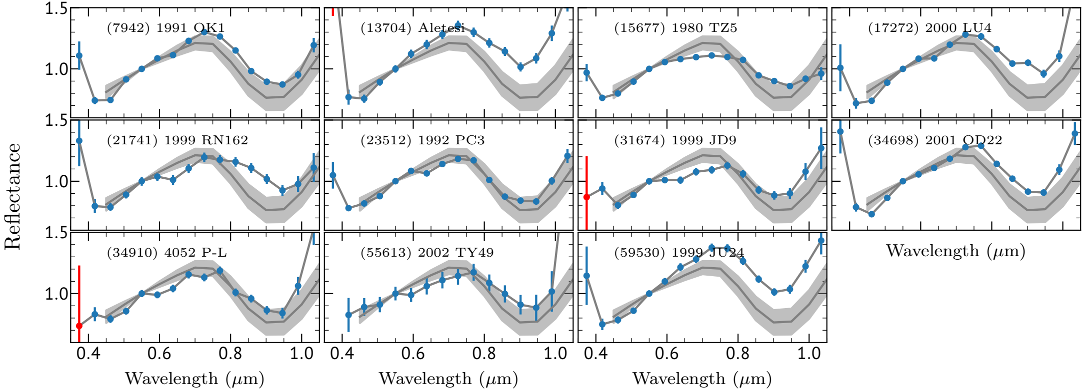

Results - spectra of predicted V-types in the middle belt

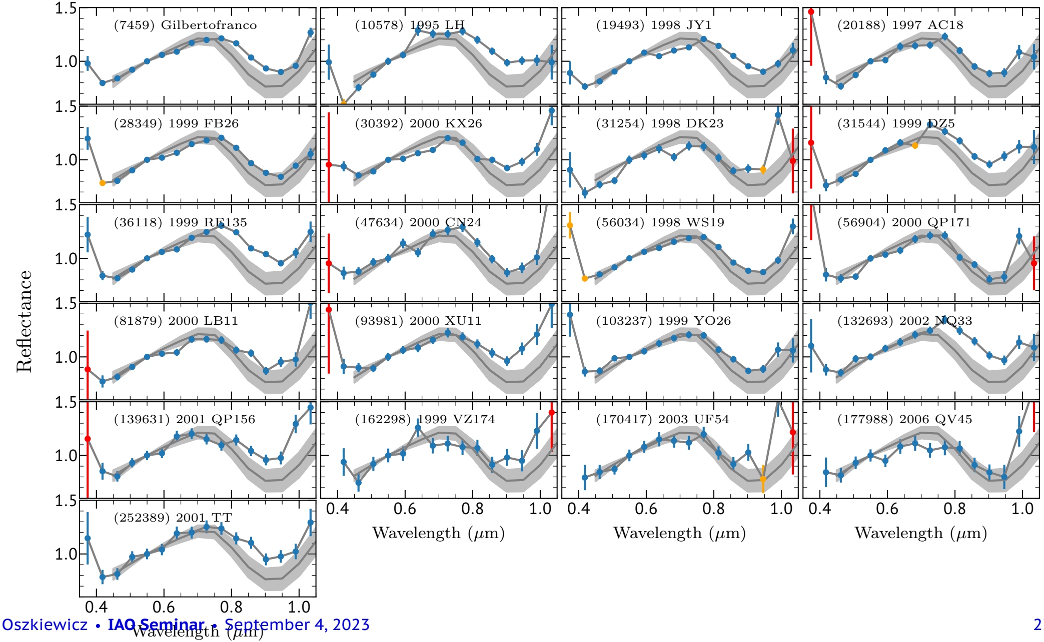

Results - spectra of predicted V-types in the Phocaea region

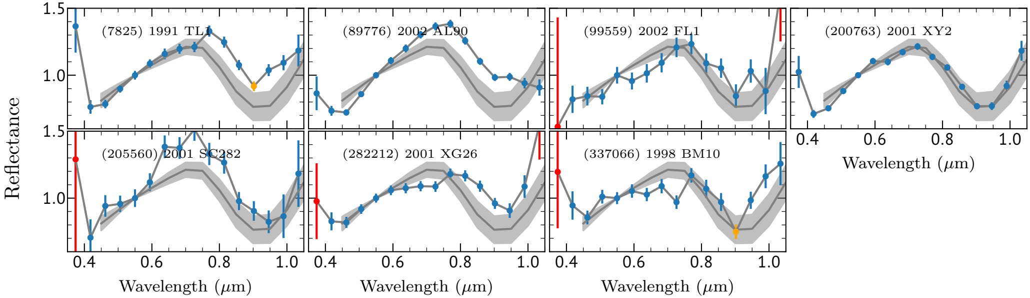

Results- spectral parameters

- Refined sample of objects with snr $>$ 40 and quality flags validated in the wavelength ranges of the investigated parameters
- Linear regression fits for wavelength ranges 0.5μm-0.75μm (red, slope A) and 0.8μm-0.92μm (orange, Slope B).
- Grey line represents fitted cubic spline, reflectances at wavelengths used in computation of band depth are denoted with stars.
- Center of the 0.9μm absorption band is denoted with a diamond symbol.
- We remove objects for which band depth is less than 1.2 from the analysis - miss-classified S-complex objects

Steeper A-slopes are an indication of space weathering and a higher band depth relates to a larger grain size, the presence of fresh/unweathered pyroxene, or a different mineralogy.

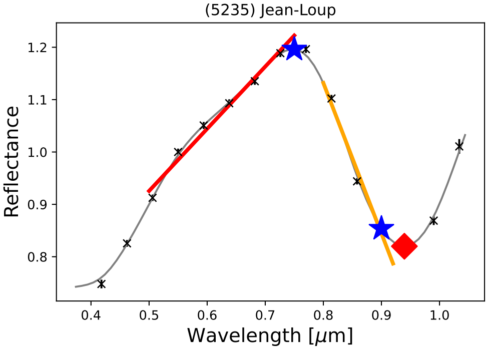

Figure: Gaia spectrum of (5235) Jean-Loup. DR3 uncertainties are on the order of marker size.

Results - spectral parameters

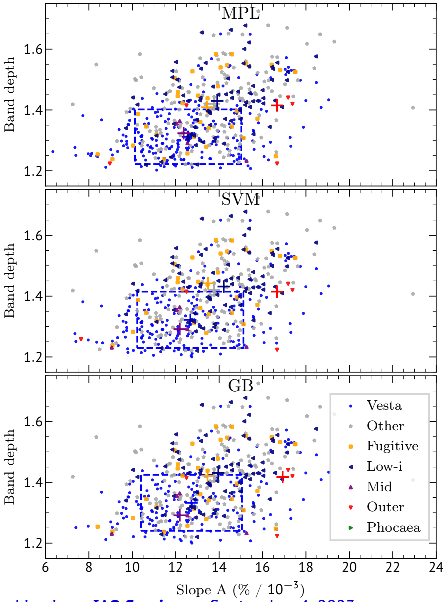

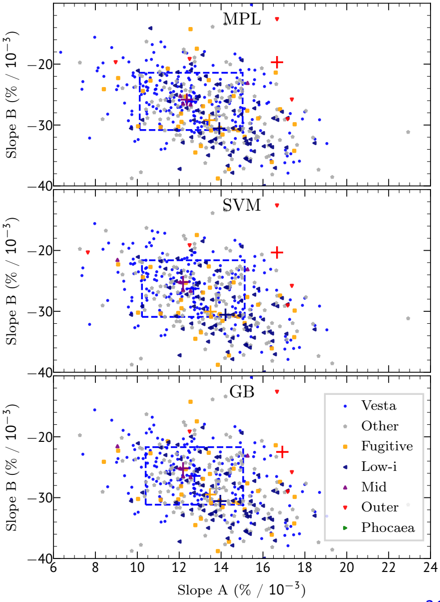

Results - spectral parameters

- Overall the median values are consistent across the different algorithms
- Outer MB, Fugitives, IO, and low-i averages are on the boarder of the 1-std envelope for the Vesta family
- Middle MB population have their average band depth and Slope A within the 1-std envelope for the dynamical Vesta family members

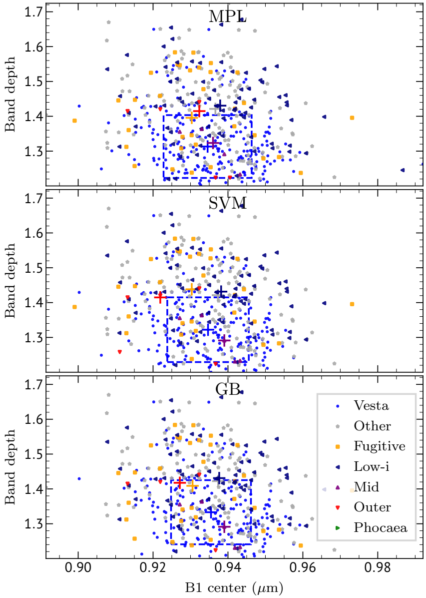

Results - spectral parameters

- While many MOVs show larger apparent depth than typical Vestoids, we also find objects (e.g. 15667 (5046 T-3) and 19493 (1998 JY1)) with a smaller band depth
- Two objects in the outer main-Belt (7942 and 34698), both at a$\sim$ 3.17 AU show similar spectral parameters indicating a plausible common origin, but numerical studies have to confirm this finding
- In the inner main-Belt, there is large variability of spectral parameters for all populations. Fugitives, low-i and inner-other populations mostly overlap with the Vesta family objects in the spectral parameters space. Yet, a number of objects from those populations have band depths well outside the 2-std envelope of the Vesta family members. Furthermore, some of the objects have band depths even greater than that of (1459) Magnya.

Searching for traces of differentiated planetesimals

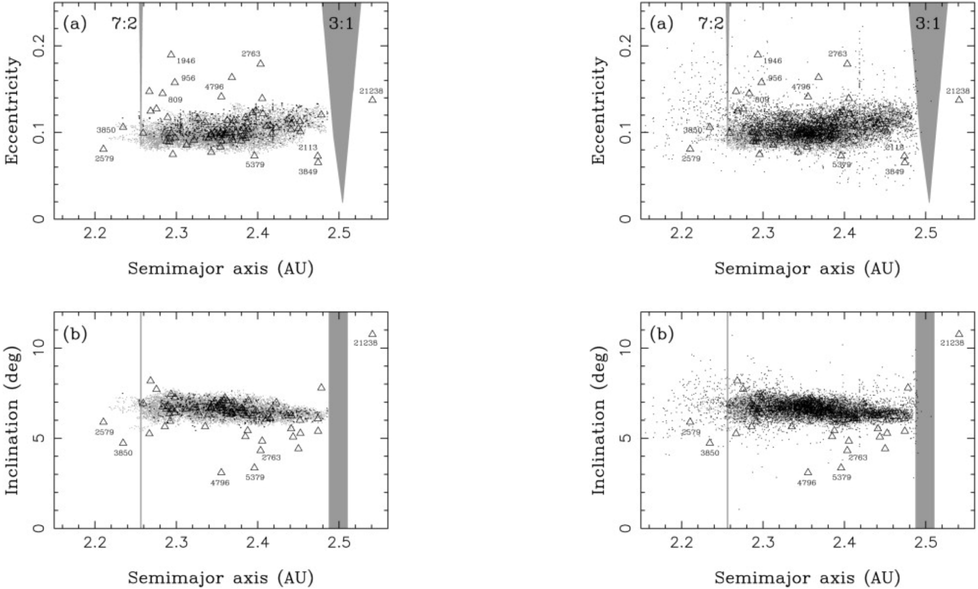

Nesvorny et al. 2008

Searching for traces of differentiated planetesimals

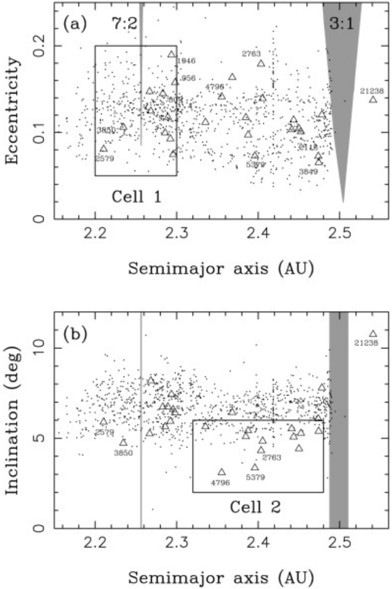

Nesvorny et al. 2008

Numerical simulations of Nesvorny et al. 2008:

- Cell I:
  - 81% retrograde
  - 19% prograde
- Cell II:
  - 40% retrograde
  - 60% prograde

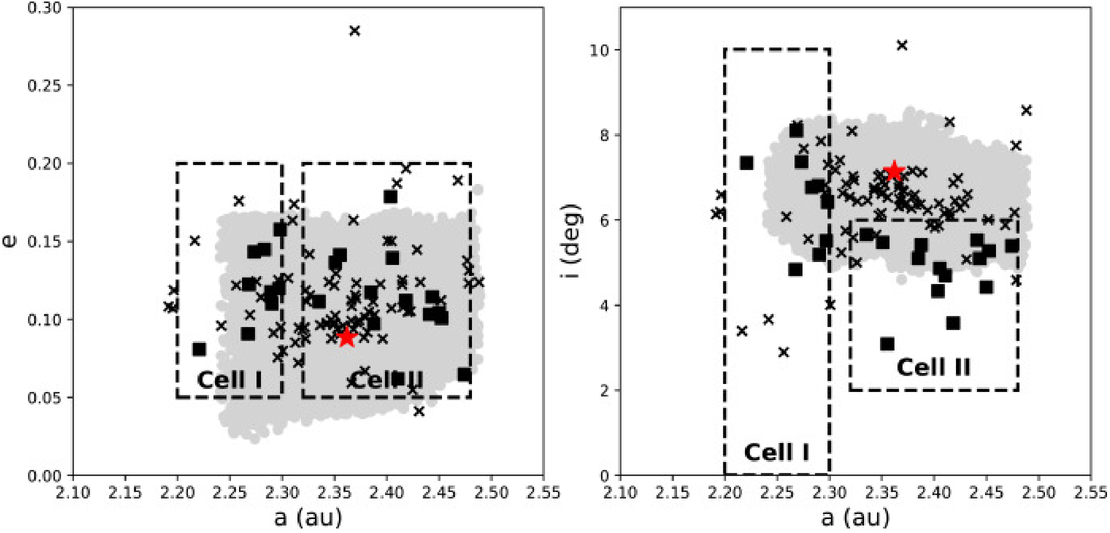

Figure: Distribution of orbital elements of observed V-types.

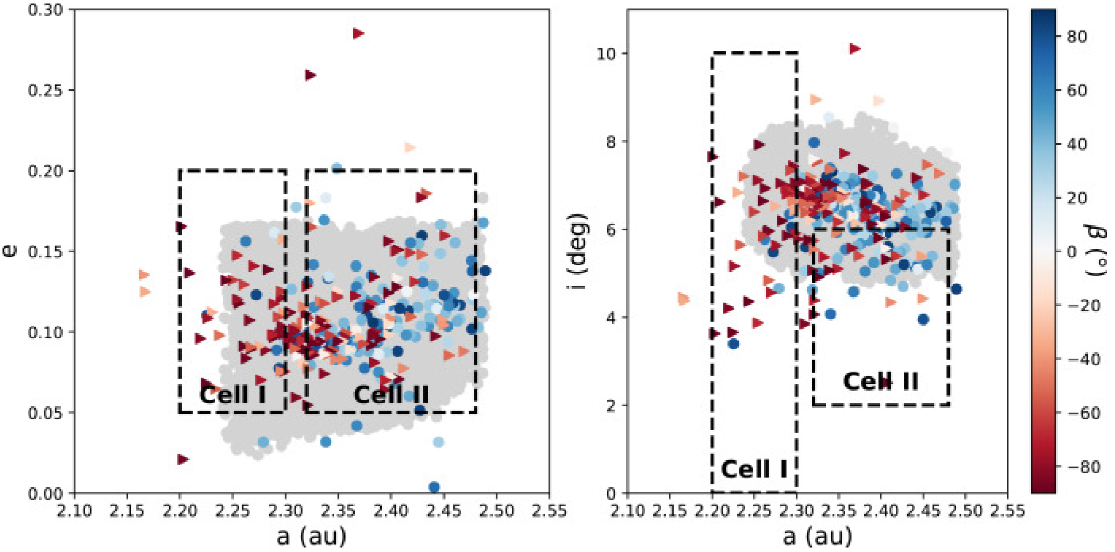

Figure: Distribution of orbital elements of studied V-types color-coded with β of the pole.

Searching for traces of differentiated planetesimals

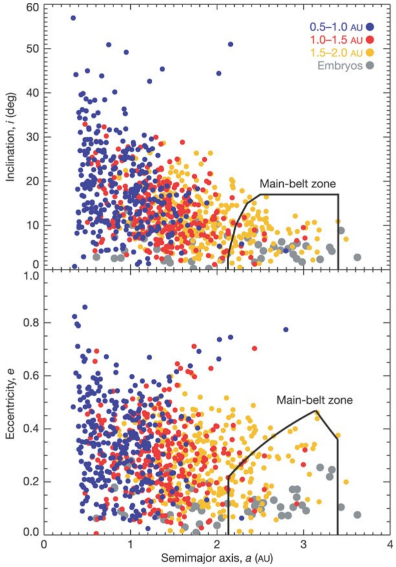

Numerical simulations (Nesvorny et al. 2008):

- Cell I:
  - 81% retrograde
  - 19% prograde
- Cell II:
  - 40% retrograde
  - 60% prograde

Observations (Oszkiewicz et al. 2023):

- Cell I:
  - 78% $\pm$11% retrograde
  - 22% $\pm$11% prograde
- Cell II:
  - 38% $\pm$13% retrograde
  - 62% $\pm$13% prograde

Parent bodies of adesitic meteorites

M. Galinier et al.: *Gaia* search for early-formed andesitic asteroidal crusts

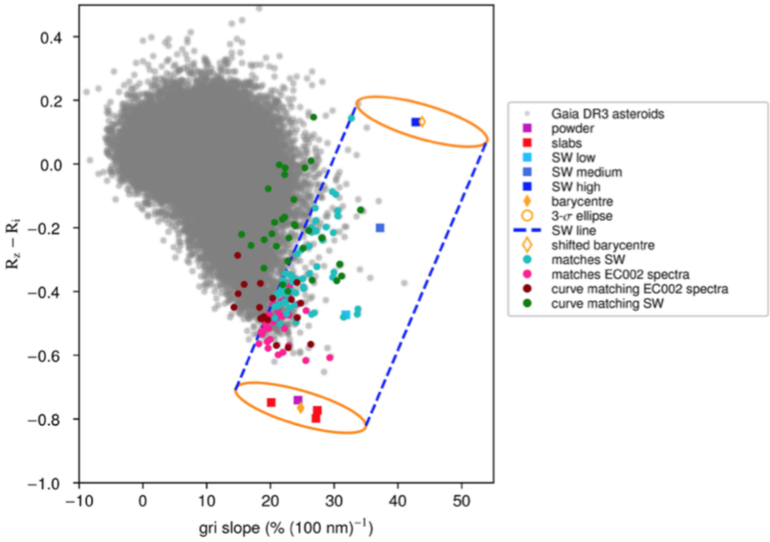

Galinier et al. 2023

Future

- The miss-match between the DR3 and ground-based spectra at red part of the spectrum are yet to be explained
- Full classification of the DR3 spectra to some(?) taxonomic scheme
- Gaia taxonomy
- investigation of spectral phase reddening/coloring, space weathering, other effects and many more
- Awaiting next Gaia releases, LSST, Euclid and others

Thank You for Your Attention!